Ionization of magnesium atoms in femtosecond 400-nm laser fields

Jie Zhou, ¹ Bradford K. Talbert, ² Yu Hang Lai ⁰, ^{3,2,*} Sha Li, ² Cosmin I. Blaga, ⁴ Pierre Agostini, ² Xu Wang ¹0, ^{1,†} and Louis F. DiMauro ² ¹Graduate School, China Academy of Engineering Physics, Beijing 100193, China ²Department of Physics, The Ohio State University, Columbus, Ohio 43210, USA ³Department of Physics, The Chinese University of Hong Kong, Hong Kong SAR, China ⁴J. R. Macdonald Laboratory, Department of Physics, Kansas State University, Manhattan, Kansas 66506, USA

(Received 23 January 2022; accepted 17 June 2022; published 30 June 2022)

Atomic magnesium (Mg) is reported to ionize more efficiently in 400-nm laser fields with circular polarization (CP) than with linear polarization. This experimental result is reproduced qualitatively by numerical solutions of a two-electron time-dependent Schrödinger equation. Theoretical analyses show that intermediate excited states play an important role during the ionization process. The 3s3p state and the 3s3d state are identified as the dominant intermediate states. The main ionization pathway is identified to be $3s^2 \rightarrow 3s3p \rightarrow 3s3d \rightarrow$ ionized states. CP laser fields are shown to be able to pump more population from the ground state to the 3s3d state, leading to more efficient ionization of the Mg atoms.

DOI: 10.1103/PhysRevA.105.063112

I. INTRODUCTION

Atomic ionization is one of the fundamental phenomena of laser-atom interaction. Especially when the laser field is strong, novel ionization processes happen that are not possible with weak laser fields. These processes include multiphoton ionization [1–4], above-threshold ionization [5–7], tunneling ionization [8–10], nonsequential double ionization [11–13], etc., which have been extensively studied in the past few decades.

As quasi-two-electron systems with rich level structures, alkaline-earth-metal atoms are ideal targets for the study of atomic ionization and electron-correlation effects [14-23]. For example, a notable experimental result was the observation of a so-called "knee structure," which is an indicator of nonsequential double ionization, in the double ionization of magnesium (Mg) with 800-nm circularly polarized (CP) laser fields [18]. This initiated quite some theoretical discussions on the mechanism of electron correlations with CP laser fields [24–30]. A recent experiment confirms that recollision is the mechanism of the observed knee structure [22], extending the applicability of the well-known recollision model [31–33].

In this article, we focus on the ionization of Mg atoms with 400-nm laser fields. An interesting and unexpected experimental result is that CP laser fields are more efficient in ionizing the Mg atoms than linearly polarized (LP) laser fields, as shown in Fig. 1. For both single ionization and double ionization, the ionization yields for CP are higher than those for LP, and the difference is more pronounced for double ionization. Around intensity 10¹³ W/cm², the difference in double ionization yields between CP and LP is about an order

of magnitude. This result is in sharp contrast to the 800-nm case, where the double-ionization yield for CP, albeit with a recollision-induced enhancement, is several orders of magnitude lower than that for LP [22].

The goal of the current article is to explain the ionization mechanism of Mg with 400-nm laser fields so as to obtain an understanding of the experimental result shown in Fig. 1. A two-electron time-dependent Schrödinger equation (TDSE) is integrated numerically and the result agrees well with the experimental result, reproducing the observed features. From a closer analysis we find that intermediate excited states play an important role during the ionization process. The 3s3p state and the 3s3d state are identified as the dominant intermediate states. Ionization happens mainly through the $3s^2 \rightarrow 3s3p \rightarrow$ $3s3d \rightarrow \text{ionized state pathway}$. CP laser fields are shown to be more efficient in pumping the population to the 3s3d state than LP laser fields. This can be understood from a closer investigation of the $3s^2$ -3s3p-3s3d three-level system. Ionization happens by absorbing one or more photons from the 3*s*3*d* state; therefore, a higher population in this state leads directly to a higher ionization probability. In particular, this effect is more significant in the case of CP fields, which could be understood by considering the angular momentum.

This article is organized as follows. In Sec. II, we explain the experimental method in obtaining the result shown in Fig. 1 and the theoretical method in numerically solving the two-electron TDSE. Numerical results, theoretical analyses, and discussions are presented in Sec. III. A conclusion is given in Sec. IV.

II. METHODS

A. Experimental methods

A commercial 800-nm, 1-kHz, 80-fs Ti:sapphire amplifier system (Spectra Physics: Spitfire Ace PA) is used in the experiments. The 400-nm beam is generated by frequency doubling

^{*}yuhanglai@cuhk.edu.hk

[†]xwang@gscaep.ac.cn

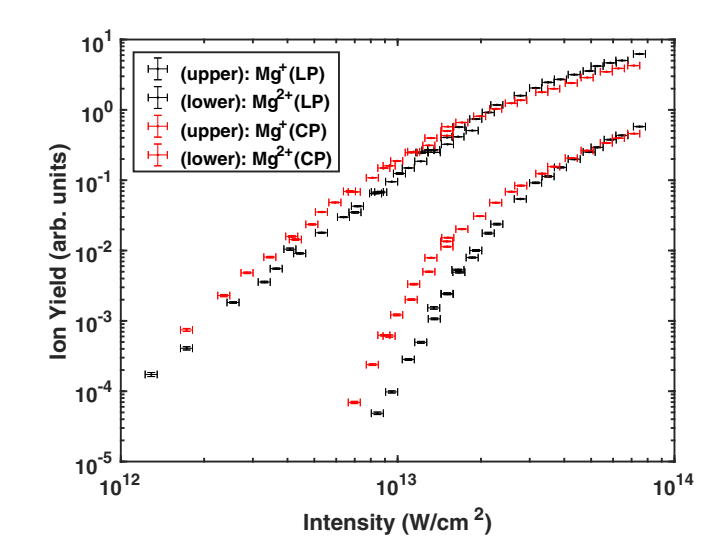


FIG. 1. Experimental ionization yields of Mg with 400-nm laser fields. For both single ionization and double ionization, yields with LP laser fields and CP laser fields are shown for comparison. The vertical error bars are given by Poisson statistics. Most of them are smaller than the size of the symbols. Horizontal error bars show the estimated fluctuation of laser intensity.

the 800-nm laser using a β -barium borate (BBO) crystal. A lens is used to focus the laser beam into a home-built time-offlight spectrometer in which ionization of atoms occurrs. An effusive source oven is mounted below the interaction region for generating a beam of Mg atoms. The laser pulse energy is controlled by an 800-nm half waveplate and polarizer placed in front of the BBO crystal. A 400-nm quarter waveplate (QWP) is placed after the BBO. To switch between LP and CP at the fixed intensity, the QWP is rotated without adjusting the laser energy. To calibrate the laser intensity, we measure the ion yield curve of a noble gas as a function of pulse energy, which is then fitted to the calculated ionization yield curve using the Perelomov-Popov-Terent'ev model [34]. To check whether the atomic density of Mg is stable over the entire period of the data-taking process, we measure the ionization yield at a particular laser intensity for several times within that period and verify that the measured yields at different times are consistent with each other.

B. Two-electron time-dependent Schrödinger equation

A Mg atom has two valence electrons and ten inner-shell electrons. For 400-nm lasers, inner-shell electrons do not participate in the ionization process since they are deeply bounded (the ionization potential of Mg²⁺ is higher than 80 eV). We use an effective ion core potential to describe the inner-shell electrons together with the nucleus. The motion of the two valence electrons in a laser field is determined by the two-body TDSE:

$$i\frac{\partial}{\partial t}\Psi(\mathbf{r}_1,\mathbf{r}_2,t) = (H_0 + H_I)\Psi(\mathbf{r}_1,\mathbf{r}_2,t). \tag{1}$$

Atomic units are used unless otherwise specified. In the above equation, the laser-free atomic Hamiltonian H_0 can be written

as

$$H_0(\mathbf{r}_1, \mathbf{r}_2) = \sum_{i=1}^{2} \left[-\frac{1}{2} \nabla_i^2 + V(r_i) \right] + V_{ee}(\mathbf{r}_1, \mathbf{r}_2), \quad (2)$$

where V is the single-electron effective potential from the ion core, and V_{ee} is an effective potential between the two valence electrons including the static Coulomb interaction and a so-called dielectronic interaction.

In our calculation the effective potential V takes the following form [35–37]:

$$V(r) = -\frac{2}{r} - \frac{A}{r}e^{-\alpha r^2} + B_l e^{-\beta_l r^2},$$
 (3)

where l is the angular momentum quantum number. The values of the parameters are given as follows (in atomic units): A = 0.583, $\alpha = 0.439$, $B_0 = 11.101$, $B_1 = 5.220$, $\beta_0 = 1.383$, and $\beta_1 = 0.995$. For l > 1, $B_l = 0$.

The effective potential V_{ee} takes the following form [38]:

$$V_{ee}(\mathbf{r}_1, \mathbf{r}_2) = \frac{1}{|\mathbf{r}_1 - \mathbf{r}_2|} - \mathbf{r}_1 \cdot \mathbf{r}_2 \sqrt{V_p(r_1)V_p(r_2)}, \quad (4)$$

where the core-polarization potential

$$V_p(r) = -\frac{\alpha_s}{2r^4} [1 - e^{-(r/R_l)^6}]. \tag{5}$$

The following parameters are used (in atomic units): $R_0 = 1.241$, $R_1 = 1.383$, and the static polarizability of the closed-shell core $\alpha_s = 0.491$.

The interaction Hamiltonian H_I in Eq. (1) is expressed in the length gauge as

$$H_I(\mathbf{r}_1, \mathbf{r}_2, t) = (\mathbf{r}_1 + \mathbf{r}_2) \cdot \mathbf{E}(t), \tag{6}$$

where $\mathbf{E}(t)$ is the laser electric field. The TDSE is solved by expanding the wave function on a basis set, which is chosen to be the eigenstates of H_0 :

$$H_0(\mathbf{r}_1, \mathbf{r}_2)\psi_{NLM}(\mathbf{r}_1, \mathbf{r}_2) = E_{NLM}\psi_{NLM}(\mathbf{r}_1, \mathbf{r}_2), \qquad (7)$$

where L and M are the quantum numbers of the total angular momentum of the two electrons, and N is a number that labels different eigenstates. Then the two-electron wave function can be expanded at any time as

$$\Psi(\mathbf{r}_1, \mathbf{r}_2, t) = \sum_{NLM} c_{NLM}(t) \psi_{NLM}(\mathbf{r}_1, \mathbf{r}_2), \tag{8}$$

and the TDSE of Eq. (1) can be rewritten as coupled differential equations of the coefficients:

$$i\frac{d}{dt}c_{NLM}(t) = E_{NLM}c_{NLM}(t) + \sum_{N'L'M'} \langle \psi_{NLM} | H_I(t) | \psi_{N'L'M'} \rangle c_{N'L'M'}(t).$$
(9)

The basis set $\psi_{NLM}(\mathbf{r}_1, \mathbf{r}_2)$ is constructed via a configuration interaction method. We first find the eigenstates of the single-electron Hamiltonian

$$H_s(\mathbf{r}) = -\frac{1}{2}\nabla^2 + V(r),\tag{10}$$

with V(r) being the potential given in Eq. (3). The eigenstates are noted as $\varphi_{nlm}(\mathbf{r})$ and they are obtained via diagonalizing

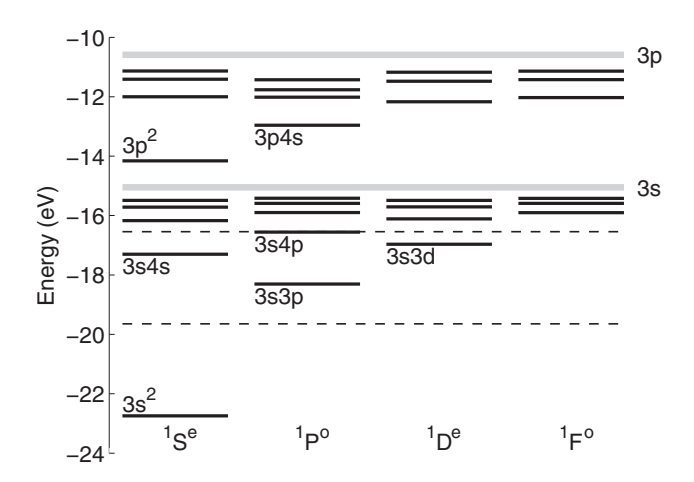


FIG. 2. Partial energy levels of the Mg atom obtained in our calculation, with Mg^{2+} as the energy reference (zero energy). The dashed lines mark one-photon and two-photon resonant energies from the $3s^2$ state with 400-nm light.

 H_s on a B-spline basis set. The following two-electron state space is constructed:

$$\phi_{n_1 n_2 LM}(\mathbf{r}_1, \mathbf{r}_2) = \sum_{l_1 l_2 m_1 m_2} \langle l_1 l_2 m_1 m_2 | LM \rangle \varphi_{n_1 l_1 m_1}(\mathbf{r}_1) \varphi_{n_2 l_2 m_2}(\mathbf{r}_2),$$
(11)

where $\langle l_1 l_2 m_1 m_2 | LM \rangle$ is the Clebsch-Gordan coefficient. Then the basis functions $\psi_{NLM}(\mathbf{r}_1, \mathbf{r}_2)$ are obtained via diagonalizing H_0 in the above state space:

$$\psi_{NLM}(\mathbf{r}_1, \mathbf{r}_2) = \sum_{n_1 n_2} a_{n_1 n_2}^{(N)} \phi_{n_1 n_2 LM}(\mathbf{r}_1, \mathbf{r}_2).$$
 (12)

For the sake of convenience, we still refer to the eigenfunctions of H_0 by common notations like 3s3p, although strictly speaking they cannot be separated into single-electron wave functions as isolated 3s and 3p states. The accuracy of the above configuration interaction method has been confirmed by experimental data in several aspects, such as the energy levels (as shown in Fig. 2) and the oscillator strengths [37,39-41].

In this article, we choose a spherical box of radius 500 a.u. and 1500 eigenstates for every (L, M) pair with the maximum L = 7. We have checked that this setting is sufficient for convergence of the performed calculations. In the beginning before turning on the laser field, the Mg atom lies in the singlet state $3s^2$. Since there is no spin-dependent term in the Hamiltonian, only singlet configurations need to be considered. The system then evolves in the presence of a 400-nm laser pulse with a trapezoidal envelope:

$$f(t) = \begin{cases} t/2T, & \text{for } t \leq 2T, \\ 1, & \text{for } 2T < t \leq 12T, \\ (14T - t)/2T, & \text{for } 12T < t \leq 14T, \end{cases}$$
 (13)

where $T = 2\pi/\omega$ is the laser period. The laser electric field has the following forms:

$$\mathbf{E}(t) = E_0 f(t) \cos(\omega t) \mathbf{e}_z, \tag{14}$$

for LP, and

$$\mathbf{E}(t) = \frac{E_0}{\sqrt{2}} f(t) [\cos(\omega t) \mathbf{e}_x - \sin(\omega t) \mathbf{e}_y], \qquad (15)$$

for CP, which is set to rotate clockwise without loss of generality.

III. NUMERICAL RESULTS AND ANALYSES

A. Ionization probabilities

The two-electron TDSEs are numerically integrated using the method described in the previous section. At the end of the laser pulse, all single-ionization (double-ionization) states can be collected to calculate the single (double) ionization probabilities. To compare with the experimental results, focal volume averaging has been performed using the experimentally estimated focal radius of 6 μ m. The theoretical results are shown in Fig. 3, together with the experimental data. One can see that the calculation results reproduce the main features observed in the experiment (Fig. 1): CP laser fields are more efficient in ionizing the Mg atom than LP laser fields. And the difference between CP and LP is more pronounced for double ionization, although the theory predicts a somewhat larger CP-LP gap for double ionization.

Note that the theory calculates the *ionization probability* of a single atom, while the experiment measures the *ion yield*, which depends on experimental conditions like the vapor pressure, the collection efficiency, etc. Therefore the absolute values of the two are not directly comparable. The relative values between the experimental data and between the theoretical curves are comparable, though. In Fig. 3 the four theoretical curves have been shifted vertically to compare with the experimental data. The curves are shifted together so the ratios between them remain fixed.

For single ionization, the dependency of the ionization probability on the laser intensity is almost a straight line (in the log-log scale) for intensities below about 10^{13} W/cm².

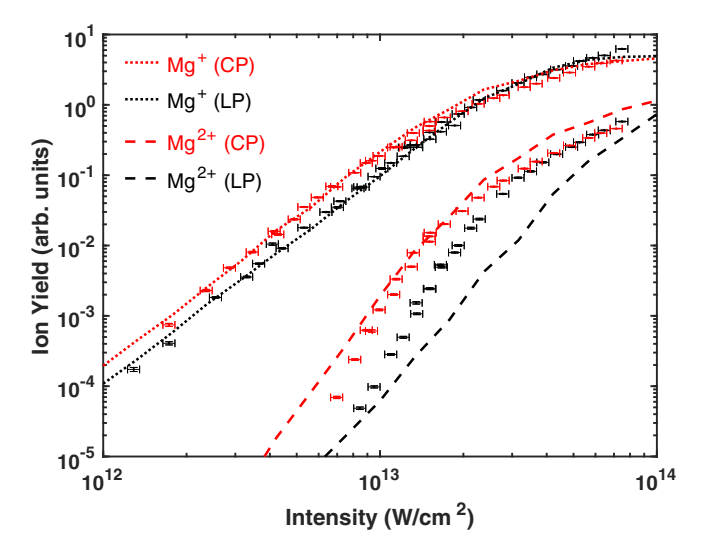


FIG. 3. Comparison between theoretical results (dotted and dashed lines) and the experimental data (points with error bars, also shown in Fig. 1). The red (gray) lines are for CP and the black lines are for LP.

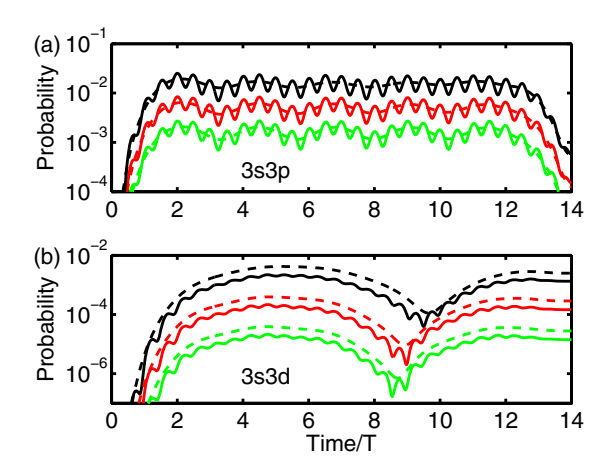


FIG. 4. Population of (a) the 3s3p state and (b) the 3s3d state during a laser pulse, for three different intensities. Top (black) curves: 10^{12} W/cm². Middle (red, gray) curves: 3.16×10^{11} W/cm². Low (green, light gray) curves: 10^{11} W/cm². For each intensity, the solid curve is for linear polarization and the dashed curve is for circular polarization.

The slope is 3, indicating a three-photon process [42,43]. This is indeed the case considering that the first ionization energy of Mg is 7.6 eV and the photon energy of 400-nm lasers is 3.1 eV. Ionization saturates with intensities above $10^{13} \, \text{W/cm}^2$.

B. The $3s^2 \rightarrow 3s3p \rightarrow 3s3d \rightarrow \text{ionization pathway}$

The calculation also records the evolution of the population of each state during the laser pulse. We find that only a few low-lying excited states, especially the 3s3p state and the 3s3d state (see Fig. 2), are noticeably occupied. Comparatively other excited states are much less occupied during the laser pulse. For example, the occupation of the 3s4p state is usually 2 orders of magnitude less than that of the 3s3p state. The 3s4d state is several times less than that of the 3s3d state. Other excited states are even less occupied.

These excited-state occupations can be understood from the energy-level diagram of Fig. 2 together with the dipole selection rule. As mentioned above, single ionization of Mg with 400-nm light is a three-photon process, and the 3s3p (3s3d) state is the lowest-energy state with angular momentum quantum number L=1 (L=2). These two states are, therefore, two important ladders through which ionization happens.

Figure 4 shows the evolution of the probability of the 3s3p state and the 3s3d state during the laser pulse, for three different intensities. For each intensity, LP (solid curves) and CP (dashed curves) cases are compared. One sees that the population of the 3s3p state is similar for LP and for CP, except for the cycle oscillations shown in LP. In contrast, the population of the 3s3d state is overall higher for CP than for LP. These results can be understood from a closer investigation of the $3s^2 - 3s3p - 3s3d$ three-level system, as is explained in the following section.

The importance of the 3s3p and the 3s3d states can be seen from Fig. 5, which shows the ion yields if these two intermediate states are removed (the same focal volume averaging and vertical shifting as in Fig. 3 have been performed). This

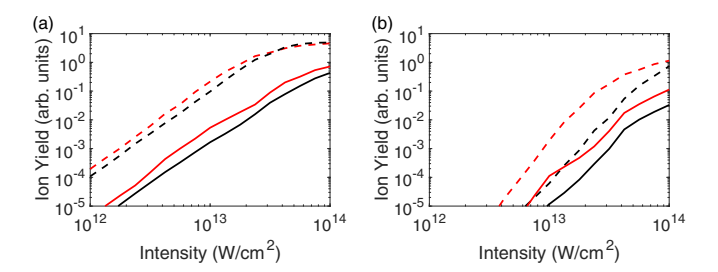


FIG. 5. Solid curves: Ion yields of the Mg atom if the 3s3p and the 3s3d states are removed from the model atom. Dashed curves: Ion yields with these two states (also shown in Fig. 3). Red (gray) curves are for CP and black curves are for LP. Panel (a) is for single ionization and panel (b) is for double ionization. Without these two states as ladders, the ionization probabilities drop for 1 to 2 orders of magnitude.

can be done in the TDSE calculation by setting to zero all the matrix elements relevant to these two states. One can see that, without these two states as ladders, the ion yields reduce by 1 to 2 orders of magnitude. In other words, the majority of ionization happens through these two excited states.

C. The $3s^2$ -3s3p-3s3d three-level system

The preference of CP in populating the 3s3d state can be understood by an investigation of the $3s^2$ -3s3p-3s3d three-level system. Simple analytical results can be obtained which agree with the numerical results shown in Fig. 4, with the aid of a rotating-wave approximation.

The 3s3p state (L=1) is degenerated with M=0 and ± 1 , and the 3s3d state (L=2) is degenerated with M=0, ± 1 , and ± 2 . According to the dipole selection rule, with the laser electric fields given in Eqs. (14) and (15), only states with M=0 are involved for LP and states with $M=\pm L$ are involved for CP. We may rewrite Eqs. (14) and (15) in the following forms:

$$\mathbf{E}(t) = \frac{E_0}{2} f(t) (e^{i\omega t} + e^{-i\omega t}) \mathbf{e}_z, \tag{16}$$

for LP, and

$$\mathbf{E}(t) = \frac{E_0}{2} f(t) (e^{i\omega t} \mathbf{e}_+ + e^{-i\omega t} \mathbf{e}_-), \tag{17}$$

for CP. Here we have made use of complex polarization vectors $\mathbf{e}_{+} = (\mathbf{e}_{x} + i\mathbf{e}_{y})/\sqrt{2}$ and $\mathbf{e}_{-} = (\mathbf{e}_{x} - i\mathbf{e}_{y})/\sqrt{2}$.

If the laser frequency ω is close to the energy gap of a transition (here the $3s^2$ -3s3p transition), then we may neglect the $e^{i\omega t}$ terms in Eqs. (16) and (17). This is a familiar rotating-wave-type approximation. Then we only need to consider the $e^{-i\omega t}$ terms, and hence only the \mathbf{e}_{-} component of CP. The ratio of the dipole transition matrix elements can be shown to be proportional to the Wigner 3-j symbols [38,44]:

$$\frac{\langle N', L+1, -L-1 | \mathbf{D} \cdot \mathbf{e}_{-} | N, L, -L \rangle}{\langle N', L+1, 0 | \mathbf{D} \cdot \mathbf{e}_{z} | N, L, 0 \rangle}$$

$$= \begin{pmatrix} L & 1 & L+1 \\ -L & -1 & L+1 \end{pmatrix} / \begin{pmatrix} L & 1 & L+1 \\ 0 & 0 & 0 \end{pmatrix}, (18)$$

where $\mathbf{D} = -(\mathbf{r}_1 + \mathbf{r}_2)$ is the dipole operator.

With the rotating-wave approximation, the evolution of the three-level system is given by

$$i\dot{c}_0(t) \approx E_0 c_0(t),\tag{19}$$

$$i\dot{c}_1(t) \approx E_1 c_1(t) + \frac{E_0}{2} f(t) e^{-i\omega t} \langle 1|\mathbf{D} \cdot \mathbf{e}_{z/-}|0\rangle c_0(t),$$
 (20)

$$i\dot{c}_2(t) \approx E_2 c_2(t) + \frac{E_0}{2} f(t) e^{-i\omega t} \langle 2|\mathbf{D} \cdot \mathbf{e}_{z/-}|1\rangle c_1(t).$$
 (21)

For simplicity we have denoted $3s^2$ state 0, 3s3p state 1, and 3s3d state 2. Besides, since most of the population still remains in the $3s^2$ state, we have neglected the feeding of state 1 to state 0 and state 2 to state 1 in these equations. Then $c_0(t) \approx e^{-iE_0t}$ and $c_1(t)$ has the following approximate solution:

$$c_1(t) \approx -i\langle 1|\mathbf{D} \cdot \mathbf{e}_{z/-}|0\rangle \int_0^t dt' \frac{E_0}{2} f(t') e^{i(E_1 - E_0 - \omega)t'}. \quad (22)$$

The time integral is the same for LP and CP, so the ratio of $c_1(t)$ between CP and LP is given by

$$\frac{c_1^{\text{CP}}(t)}{c_1^{\text{LP}}(t)} \approx \begin{pmatrix} 0 & 1 & 1\\ 0 & -1 & 1 \end{pmatrix} / \begin{pmatrix} 0 & 1 & 1\\ 0 & 0 & 0 \end{pmatrix} = -1. \tag{23}$$

This explains the results of Fig. 4(a) that the population of the 3s3p state is similar for LP and CP (except for the fast cycle oscillations shown in LP). Similarly, we find that

$$\frac{c_2^{\text{CP}}(t)}{c_2^{\text{LP}}(t)} \approx \frac{c_1^{\text{CP}}(t)}{c_1^{\text{LP}}(t)} \begin{pmatrix} 1 & 1 & 2 \\ -1 & -1 & 2 \end{pmatrix} / \begin{pmatrix} 1 & 1 & 2 \\ 0 & 0 & 0 \end{pmatrix} = -\sqrt{\frac{3}{2}}.$$
(24)

This means that CP pumps 1.5 times the population from the ground $3s^2$ state to the 3s3d state than LP does, agreeing well with the numerical results shown in Fig. 4(b).

We may go a little further beyond the above three-level model and extend the deduction to continuum states with energy $E_L = E_{L-1} + \omega$ and angular quantum numbers (L, -L) for CP and (L, 0) for LP. The result is

$$\frac{c_L^{\text{CP}}(t)}{c_L^{\text{LP}}(t)} \approx \frac{c_{L-1}^{\text{CP}}(t)}{c_{L-1}^{\text{LP}}(t)} \binom{L-1}{-L} \quad \frac{1}{-1} \quad \frac{L+1}{L+1} \bigg) \bigg/ \binom{L-1}{0} \quad \frac{1}{0} \quad 0 \bigg)$$

$$= (-1)^{L} \sqrt{\frac{2L-1}{L}} \frac{c_{L-1}^{\text{CP}}(t)}{c_{L-1}^{\text{LP}}(t)}.$$
 (25)

We can see that the ratio of population between CP and LP increases with L or, equivalently, with the number of the photons absorbed. The ratio, for example, is 1.5 for L=2 and 2.5 for L=3, agreeing also with an analysis obtained in Ref. [45].

D. Energy distribution of ionized states

The 3s3d state plays a particularly important role in the ionization of Mg atoms with 400-nm laser fields. Ionization happens by absorbing one or more photons from the 3s3d state. This assessment can be clearly seen from Fig. 6, which shows the energy distribution of ionized states, including both singly ionized states and doubly ionized states. The vertical dashed line near the left end of the figure marks the energy of the 3s3d state. The leftmost peak of singly ionized states

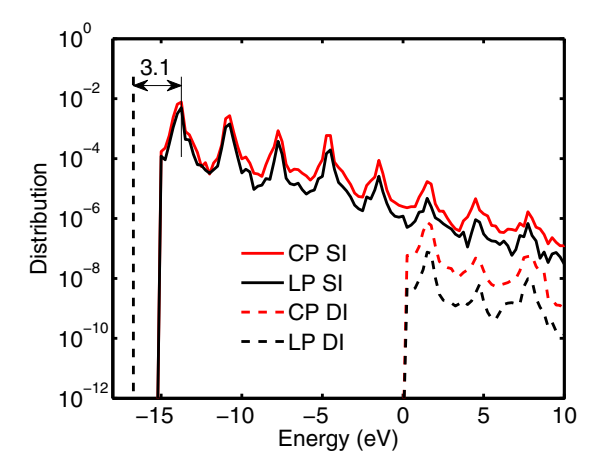


FIG. 6. Population of ionized states induced by LP (black) or CP (red, gray) pulses of intensity 10^{12} W/cm². Solid curves are for single ionization and dashed curves are for double ionization.

is one photon (3.1 eV) from the 3s3d state. Peaks with higher energies are separated by the photon energy, corresponding to multiphoton absorption from the 3s3d state.

Double ionization also originates from multiphoton absorptions from the 3s3d state. This can be seen from the observation that the peaks of doubly ionized states locate at the same positions as the corresponding single-ionization peaks. A minimum number of six photons are needed to doubly ionize the Mg atom from the 3s3d state.

One also sees that for both single ionization and double ionization, CP is more effective in ionizing the Mg atom than LP. In addition, one can see the trend that the higher the energy, the larger the separation between these two polarizations. The difference between CP and LP for double ionization is more pronounced than that for single ionization, corresponding to the results shown in Figs. 1 and 3.

E. Further remarks

On the role of recollision in double ionization. Recollision is an important process in atomic double ionization. Especially for Mg, with 800-nm laser fields, recollision happens even with CP laser fields [18,22]. For 400-nm laser fields, however, it is not difficult to see that recollision plays a negligible role. The quiver motion amplitude of a free electron in a laser electric field is $\Delta x = E_0/\omega^2$. For recollision to be a sensible concept, this quiver motion amplitude should be much larger than the size of the atom itself. For an intensity of 10^{13} W/cm² and a wavelength of 400 nm, one gets $\Delta x \approx 1.3$ a.u., which is merely the size of the atom. For an intensity of 10¹⁴ W/cm², $\Delta x \approx 4.1$ a.u., which is merely two or three times the size of the atom. From the energy perspective, the maximum recollision energy is $3.17U_p = 3.17E_0^2/4\omega^2$, which is 0.47 eV for 10^{13} W/cm² and 4.7 eV for 10^{14} W/cm², both being much lower than the second ionization potential of Mg (15 eV). Therefore, we can conclude that the recollision process plays a negligible role in the double ionization of Mg with 400-nm laser fields.

On the $3s^2 \rightarrow 3s3p \rightarrow 3s3d \rightarrow ionization pathway$. Identifying a dominant and relatively simple ionization pathway is not always possible. In general, the ionization process is so

complicated that a large number of pathways participate and no single pathway dominates. For the Mg atom and 400-nm laser fields, the 3s3p state is relatively close to one-photon resonance and the 3s3d state is relatively close to two-photon resonance from the $3s^2$ ground state (see Fig. 2). This somewhat lucky condition allows the existence of a dominant ionization pathway. This condition, however, does not hold for other wavelengths, such as 800 nm. Neither does it hold for other alkaline-earth-metal atoms in 400-nm laser fields. Ionization of Mg in 400-nm laser fields is a special case that renders theoretical analyses relatively simple.

IV. CONCLUSION

In this joint experimental and theoretical article, we have reported experimental results on the ionization of Mg atoms with 400-nm laser fields. CP laser fields are found to be more efficient in ionizing the Mg atom than LP laser fields, in sharp contrast to previous ionization results with 800-nm laser fields [22].

To understand these experimental results, we have performed a two-electron TDSE calculation. The numerical results agree well with the experimental results and reproduce the main observed features. Careful analyses allow the identification of a dominant ionization pathway, namely, the

- $3s^2 \rightarrow 3s3p \rightarrow 3s3d \rightarrow$ ionization pathway. CP laser fields are shown to be more efficient in pumping the population from the ground state to the 3s3d state than LP laser fields. A simplified three-level model has been used to make sense of this CP preference. Ionization happens by absorbing one or more photons from the 3s3d state, so more population in this state leads to higher probabilities of ionization.
- Our results provide a manifestation of resonant intermediate states on strong-field multiphoton ionization. It would be interesting to see new and possibly unexpected manifestations with different alkaline-earth-metal atoms and/or laser parameters.

ACKNOWLEDGMENTS

We acknowledge grants from the National Natural Science Foundation of China under Grants No. 11774323, No. 12004380, and No. 12088101; the Science Challenge Project of China under Grant No. TZ2018005; and the NSAF under Grant No. U1930403. The DiMauro Group acknowledges funding support from the U.S. National Science Foundation under Grant No. 1605042. C.I.B. acknowledges financial support by the U.S. Department of Energy (DOE), Office of Science, Basic Energy Sciences (BES), under Grant No. DE-FG02-86ER13491.

- [1] L. V. Keldysh, Sov. Phys. JETP 20, 1307 (1965).
- [2] G. Voronov and N. Delone, JETP Lett. 1, 66 (1965).
- [3] P. Agostini, G. Barjot, J. F. Bonnal, G. Mainfray, and C. Manus, IEEE J. Quantum Electron. 4, 667 (1968).
- [4] G. Mainfray and C. Manus, Rep. Prog. Phys. 54, 1333 (1991).
- [5] P. Agostini, F. Fabre, G. Mainfray, G. Petite, and N. K. Rahman, Phys. Rev. Lett. 42, 1127 (1979).
- [6] P. Kruit, J. Kimman, H. G. Muller, and M. J. van der Wiel, Phys. Rev. A 28, 248 (1983).
- [7] G. G. Paulus, W. Nicklich, H. Xu, P. Lambropoulos, and H. Walther, Phys. Rev. Lett. 72, 2851 (1994).
- [8] M. V. Ammosov, N. B. Delone, and V. P. Krainov, Sov. Phys. JETP **64**, 1191 (1986).
- [9] S. L. Chin, F. Yergeau, and P. Lavigne, J. Phys. B **18**, L213
- [10] S. L. Chin, Y. Liang, J. E. Decker, F. A. Ilkov, and M. Ammosov, J. Phys. B 25, L249 (1992).
- [11] B. Walker, B. Sheehy, L. F. DiMauro, P. Agostini, K. J. Schafer, and K. C. Kulander, Phys. Rev. Lett. 73, 1227 (1994).
- [12] S. Palaniyappan, A. DiChiara, E. Chowdhury, A. Falkowski, G. Ongadi, E. L. Huskins, and B. C. Walker, Phys. Rev. Lett. 94, 243003 (2005).
- [13] W. Becker, X. J. Liu, P. J. Ho, and J. H. Eberly, Rev. Mod. Phys. 84, 1011 (2012).
- [14] L. F. DiMauro, D. Kim, M. W. Courtney, and M. Anselment, Phys. Rev. A 38, 2338 (1988).
- [15] D. Kim, S. Fournier, M. Saeed, and L. F. DiMauro, Phys. Rev. A 41, 4966 (1990).
- [16] N. J. van Druten, R. Trainham, and H. G. Muller, Phys. Rev. A 50, 1593 (1994).

- [17] D. Xenakis, N. E. Karapanagioti, D. Charalambidis, H. Bachau, and E. Cormier, Phys. Rev. A 60, 3916 (1999).
- [18] G. D. Gillen, M. A. Walker, and L. D. Van Woerkom, Phys. Rev. A 64, 043413 (2001).
- [19] I. Liontos, A. Bolovinos, S. Cohen, and A. Lyras, Phys. Rev. A 70, 033403 (2004).
- [20] Y. H. Lai, J. Xu, U. B. Szafruga, B. K. Talbert, X. Gong, K. Zhang, H. Fuest, M. F. Kling, C. I. Blaga, P. Agostini, and L. F. DiMauro, Phys. Rev. A 96, 063417 (2017).
- [21] H. P. Kang, S. Chen, Y. L. Wang, W. Chu, J. P. Yao, J. Chen, X. J. Liu, Y. Cheng, and Z. Z. Xu, Phys. Rev. A 100, 033403 (2019).
- [22] Y. H. Lai, X. Wang, Y. Li, X. Gong, B. K. Talbert, C. I. Blaga, P. Agostini, and L. F. DiMauro, Phys. Rev. A 101, 013405 (2020).
- [23] A. Dimitriou, V. Loriot, A. Marciniak, T. Barillot, S. Danakas, F. Lepine, C. Bordas, and S. Cohen, Phys. Rev. A 105, 053106 (2022).
- [24] X. Wang and J. H. Eberly, Phys. Rev. Lett. 105, 083001 (2010).
- [25] F. Mauger, C. Chandre, and T. Uzer, Phys. Rev. Lett. 105, 083002 (2010).
- [26] X. Wang and J. Eberly, New J. Phys. 12, 093047 (2010).
- [27] L. B. Fu, G. G. Xin, D. F. Ye, and J. Liu, Phys. Rev. Lett. 108, 103601 (2012).
- [28] A. Kamor, F. Mauger, C. Chandre, and T. Uzer, Phys. Rev. Lett. 110, 253002 (2013).
- [29] J. Guo, X.-S. Liu, and S.-I Chu, Phys. Rev. A **88**, 023405 (2013).
- [30] Y. Li, B. Yu, Q. Tang, X. Wang, D. Hua, A. Tong, C. Jiang, G. Ge, Y. Li, and J. Wan, Opt. Express 24, 6469 (2016).

- [31] K. C. Kulander, K. J. Schafer, and J. L. Krause, in *Super-Intense Laser-Atom Physics*, edited by B. Piraux, A. L'Huillier, and K. Rzazewski (Plenum, New York, 1993).
- [32] K. J. Schafer, B. Yang, L. F. DiMauro, and K. C. Kulander, Phys. Rev. Lett. **70**, 1599 (1993).
- [33] P. B. Corkum, Phys. Rev. Lett. 71, 1994 (1993).
- [34] A. M. Perelomov, V. S. Popov, and M. V. Terent'ev, Sov. Phys. JETP 23, 924 (1966).
- [35] H. Preuss, H. Stoll, U. Wedig, and T. Krüger, Int. J. Quantum Chem. 19, 113 (1981).
- [36] R. Moccia and P. Spizzo, Phys. Rev. A 39, 3855 (1989).
- [37] G. Buica and T. Nakajima, J. Quant. Spectrosc. Radiat. Transfer 109, 107 (2008).

- [38] L. A. A. Nikolopoulos, Comput. Phys. Commun. 150, 140 (2003).
- [39] T. N. Chang and Y. S. Kim, Phys. Rev. A 34, 2609 (1986).
- [40] K. Aashamar, Phys. Scr. 34, 386 (1986).
- [41] R. Moccia and P. Spizzo, J. Phys. B 21, 1133 (1988).
- [42] T. Nakajima and G. Buica, Phys. Rev. A 74, 023411 (2006).
- [43] P. Lambropoulos, L. A. A. Nikolopoulos, and M. G. Makris, Phys. Rev. A 72, 013410 (2005).
- [44] I. Sobel'man, *Introduction to the Theory of Atomic Spectra* (Pergamon, Oxford, 1972).
- [45] P. Lambropoulos, Phys. Rev. Lett. 28, 585 (1972).